Holey fiber design for single-polarization single-mode guidance

Dora Juan Juan Hu,[1,*] Ping Shum,[1] Chao Lu,[2] Xia Yu,[3] Guanghui Wang,[1] and Guobin Ren[4]

[1]School of Electrical and Electronic Engineering, Nanyang Technological University, 50 Nanyang Avenue, Singapore 639798

[2]Department of Electronic and Information Engineering, Hong Kong Polytechnic University, Hong Hom, Kowloon, Hong Kong

[3]Singapore Institute of Manufacturing Technology, 71 Nanyang Drive, Singapore 638075

[4]College of Science, The Central University for Nationalities, Beijing 100081, China

*Corresponding author: hujuanjuan@pmail.ntu.edu.sg

We propose a holey fiber design to achieve single-polarization single-mode (SPSM) guidance. The photonic crystal fiber (PCF) has a triangular-lattice with elliptical airholes in the microstructured cladding and circular airholes in the core. The SPSM guidance can be obtained by designing the PCF structure such that the fundamental space-filling mode (FSM) of the core region is positioned between the indices of the two nondegenerate orthogonally polarized FSMs of the microstructured cladding. © 2009 Optical Society of America

OCIS codes: 060.0060, 060.5295.

1. Introduction

A single-polarization single-mode (SPSM) fiber guides only one polarization mode and thus eliminates mode coupling between the two orthogonally polarized fundamental modes. This is an important feature for polarization-sensitive applications such as high-power fiber lasers, fiber-optic gyroscopes, current sensors, and superluminescent sources [1]. Compared with polarization-maintaining (PM) fibers that support two orthogonal polarization states, a SPSM fiber offers several advantages including a high extinction ratio, no polarization mode dispersion, and polarization-dependent loss issues. To achieve SPSM guidance, the fiber is designed with the effective index of the desired polarization above the effective index of the cladding, and the effective index of the undesired polarization is well below that of the cladding. SPSM fibers have been designed and used by conventional optical fibers with an elliptical core or a bow-tie structure or different polarization-dependent loss along the two orthogonal axes [2–6]. With the development of photonic crystal fibers (PCFs) that have periodic arrays of airholes running along the fiber axis, a remarkable design freedom on waveguiding properties is exploited such as broadband single-mode operation [7], unusual dispersion properties [8], and high birefringence [9,10]. For PCFs with a triangular lattice of airholes, by breaking the sixfold symmetry [11], e.g., having different airhole diameters along the two orthogonal axes, high birefringence is easily produced. Recently, it has been demonstrated that SPSM guidance can be achieved by use of hole-assisted fibers and high-birefringent PCFs [12–22]. It has been numerically studied [21,22] that the SPSM can be achieved by designing the FSM for a circular-hole holey structure to lie between the anisotropic FSM for the elliptical-hole core.

We report a novel triangular-lattice PCF-based structure to achieve SPSM operation and numerically study its waveguiding properties by using a full-vector plane-wave expansion (PWE) method and finite element method (FEM). The core region contains a circular-hole holey structure and the cladding region consists of an elliptical airhole triangular lattice structure. The FSM of the circular-hole core is designed between the anisotropic FSMs of the elliptical-hole cladding so that SPSM guidance is supported. We theoretically investigate the influence of the PCF structural parameters such as the geometry of the core and the cladding on the properties of SPSM operation. The single polarization regions and cutoff conditions for higher-order modes are discussed.

2. Design and Analysis

The schematic design of the PCF structure is depicted in Fig. 1. The core consists of multiple defects of circular airholes surrounded by a triangular-latticed cladding with elliptical airholes. The structural parameters of the PCF are as follows. The lattice pitch is denoted as Λ, the circular airholes in the core region have a relative diameter of d_c/Λ, and the elliptical airholes in the cladding regions have a relatively long axis length of d_y/Λ and ellipticity of $\eta = d_y/d_x$. The background medium is fused silica with refractive index $n_{SiO_2} = 1.45$. It should be noted that in a typical index-guiding PCF in which the defect core is missing an airhole [7], the guidance is found in the wavelength region where the core index, i.e., the silica refractive index, is higher than that of the FSM of the microstructured cladding. However, because of the sixfold symmetry of the structure, two polarizations of the fundamental mode, HE_{11}^x and HE_{11}^y, are degenerate and therefore the PCF is not truly single mode. Comparatively, the sixfold symmetry of the proposed PCF is broken by the elliptical airholes in the cladding that behave like an anisotropic medium. The two orthogonally polarized
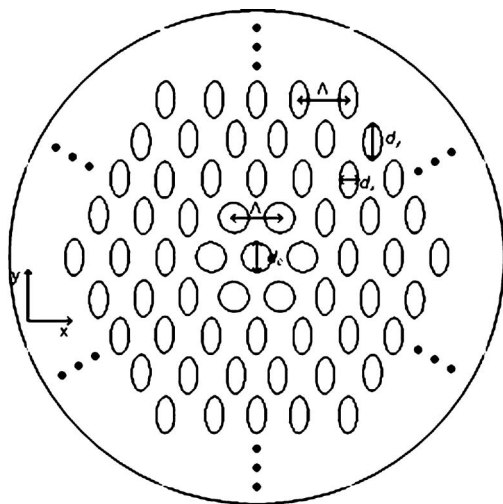
FSMs of the cladding become nondegenerate, and they provide the cutoff of guided modes in the infinite lattice. The FSM of the core region can be designed with suitable airhole geometry so that it is positioned between the two FSMs of the cladding, i.e., only one polarization can be guided in the core.

We use the full-vector PWE method to calculate the effective index of the FSMs of the microstructures. As shown in Fig. 2, the effective index n_{eff} of the FSMs for the circular airhole lattice (denoted as FSM_c) at $d_c/\Lambda = 0.62$ (dotted curve), 0.64 (solid curve), and 0.66 (dashed curve), and the elliptical airhole lattice (the FSM curve for the y-polarized cladding mode denoted as FSM_e^y and the FSM curve for the x-polarized cladding mode denoted as FSM_e^x) are calculated versus the normalized wavelength λ/Λ. The other parameters of the PCF structures are as follows: $d_y/\Lambda = 0.9$ and $\eta = 2$. As d_c/Λ increases, the n_{eff} of the FSM_c curve decreases to lower values versus normalized wavelength λ/Λ. In addition, the intersecting points with the FSM curves of the cladding, which are important parameters to define the single polarization operating range, also change. In the wavelength range where the FSM_c curve lies below the FSM_e^y curve and above the FSM_e^x curve, only the x-polarized mode is guided in the core region by the PCF structure. The corresponding normalized cutoff wavelengths for the HE_{21}^x mode are 1.01, 0.3, and 0.75, respectively. In Fig. 3, the operating map shows the wavelengths of the single-polarization guidance as a function of d_c/Λ. The single-polarization region is defined by the area within the solid curve. Moreover, the SPSM operation is achieved by cutting off the higher-order mode, i.e., the next higher-order mode is HE_{21}^x, and its cutoff wavelength is represented by a dashed curve.

Next we examine the influence of ellipticity η on the SPSM operating properties. We use $d_c/\Lambda = 0.63$ and $d_y/\Lambda = 0.9$, and η varies from 1.9 to 2.1.

Fig. 1. Cross section of the proposed PCF with elliptical airhole cladding and a circular hole core.
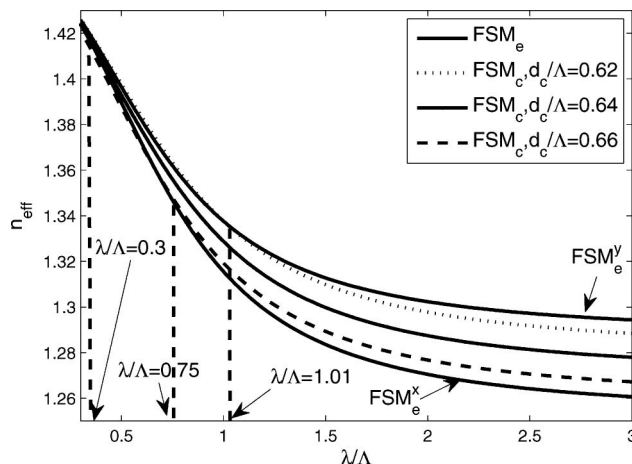

Fig. 2. Effective index of the FSM curves of the circular airhole core FSM_c at $d_c/\Lambda = 0.62$, 0.64, 0.66 and the two orthogonal nondegenerate FSM curves of the elliptical airhole cladding, FSM_e^x and FSM_e^y. The other structural parameters of the PCF are $d_y/\Lambda = 0.9$ and $\eta = 2$.
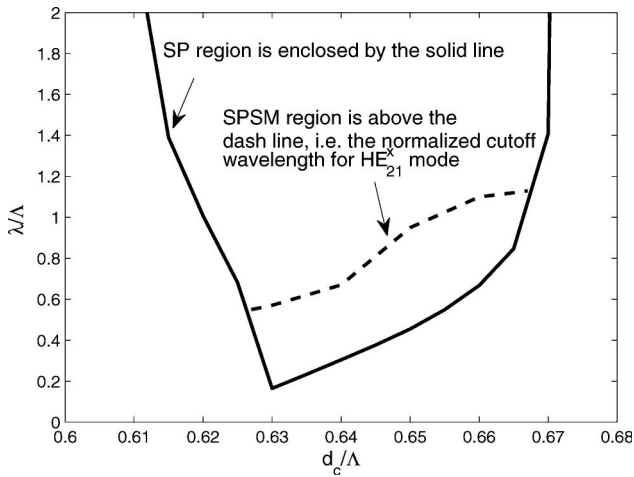
Fig. 3. Single-polarization guidance region as a function of d_c/Λ. The SPSM operation is possible above the cutoff wavelength of the HE_{21}^x mode (dashed curve) in the single polarization range. The other structural parameters of the PCF are $d_y/\Lambda = 0.9$ and $\eta = 2$.
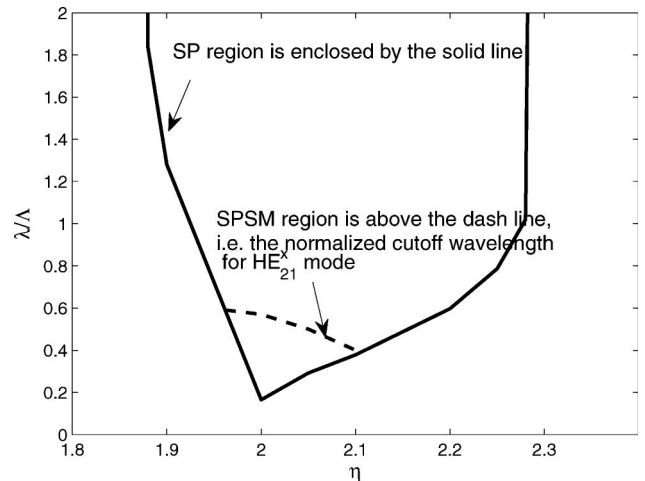

Fig. 5. Single-polarization guidance region as a function of η. The SPSM operation is possible above the cutoff wavelength of the HE_{21}^x mode (dashed curve) in the single-polarization range. The other structural parameters of the PCF are $d_y/\Lambda = 0.9$ and $d_c/\Lambda = 0.63$.

As shown in Fig. 4, the n_{eff} of the FSMs for the elliptical airhole lattice at $\eta = 1.9$ (dotted curve), 2.0 (solid curve), and 2.1 (dashed curve) increase to higher values when η increases. Effective index n_{eff} of the FSMs for the circular airhole lattice at $d_c/\Lambda = 0.63$ is represented as the solid dot line. The corresponding normalized cutoff wavelengths for the HE_{21}^x mode are 1.28, 0.17, and 0.38, respectively. In Fig. 5, the operating map shows the wavelengths of the single-polarization guidance as a function of η. Single polarization is permitted in the area within the solid curve; the dashed curve represents the normalized cutoff wavelength for the HE_{21}^x mode.

The structural parameter d_y/Λ also plays a role in determining the SPSM operating range. By setting $d_c/\Lambda = 0.63$ and $\eta = 2$, we calculate the effective index of the FSM curves for the core and cladding regions while altering d_y/Λ. As shown in Fig. 6, the n_{eff} of the FSMs for the elliptical airhole lattice at $d_y/\Lambda = 0.88$ (dotted curve), 0.9 (solid curve), and 0.92 (dashed curve) decreases to lower values when d_y/Λ

increases. Effective index n_{eff} of the FSMs for the circular airhole lattice at $d_c/\Lambda = 0.63$ is represented as the solid dotted curve. The corresponding normalized cutoff wavelengths for the HE_{21}^x mode are 0.35, 0.17, and 0.94, respectively. In Fig. 7, the operating map shows the wavelengths of the single-polarization guidance as a function of d_y/Λ. The permitted single polarization is within the solid curve; the dashed curve represents the normalized cutoff wavelength for the HE_{21}^x mode.

It is observed from Figs. 3, 5, and 7 that the single polarization operating region expands when λ/Λ increases, which is due to higher birefringence of the elliptical hole at longer wavelengths [22]. We calculate the fundamental mode of the single-polarization state with PCF structural parameters: $d_y/\Lambda = 0.63$, $\eta = 2$, and $d_y/\Lambda = 0.9$. The full-vector FEM is used to
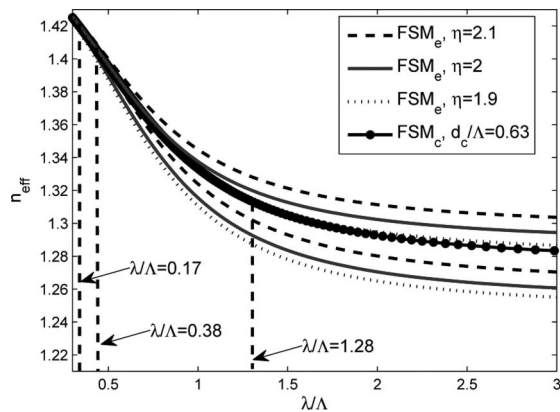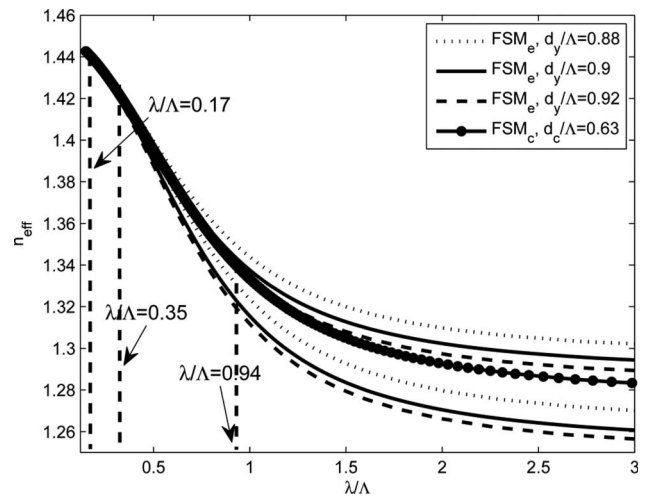

Fig. 4. Effective index of the FSM curves of the elliptical airhole cladding FSM_e at $\eta = 1.9, 2, 2.1$ and the FSM curve of the circular airhole core at $d_c/\Lambda = 0.63$. The other structural parameter of the PCF is $d_y/\Lambda = 0.9$.

Fig. 6. Effective index of the FSM curves of the elliptical airhole cladding FSM_e at $d_y/\Lambda = 0.88$ (dotted curve), 0.9 (solid curve), and 0.92 (dashed curve) and the FSM curve of the circular airhole core at $d_c/\Lambda = 0.63$ (solid dot line). $\eta = 2$ was used in the simulation.
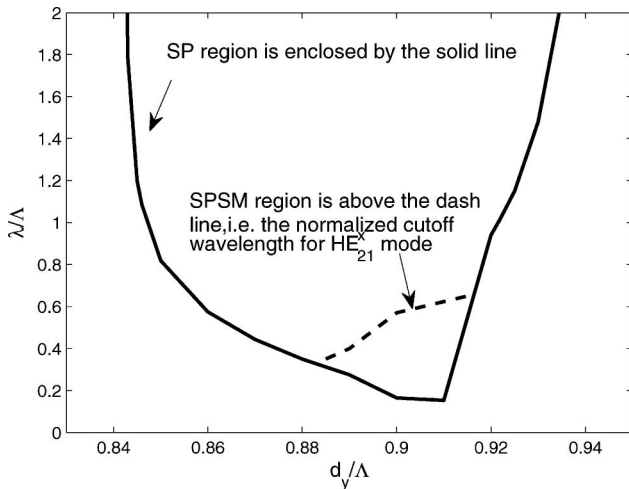
Fig. 7. Single-polarization guidance region as a function of d_y/Λ. The SPSM operation is possible above the cutoff wavelength of the HE_{21}^x mode (dashed curve) in the single-polarization range. The other structural parameters of the PCF are $\eta = 2$ and $d_c/\Lambda = 0.63$.

calculate the effective index of the x-polarized fundamental mode HE_{11}^x and is represented as the filled circles curve between the FSM_c curve and the FSM_e^x curve in Fig. 8. At long wavelengths, the effective index curve of HE_{11}^x approaches the FSM_e^x curve. The single-mode operation is achieved by cutting off the higher-order mode, and its cutoff wavelength for the HE_{21}^x mode is found at $\lambda/\Lambda = 0.57$. Therefore, broadband single-polarization guidance is obtained, and the SPSM operation is supported by this PCF structure at a λ/Λ wavelength range greater than 0.57. The field distribution of the E_x component of the x-polarized fundamental mode HE_{11}^x is plotted at $\lambda/\Lambda = 0.5$ and 1.4 wavelengths in Fig. 9.

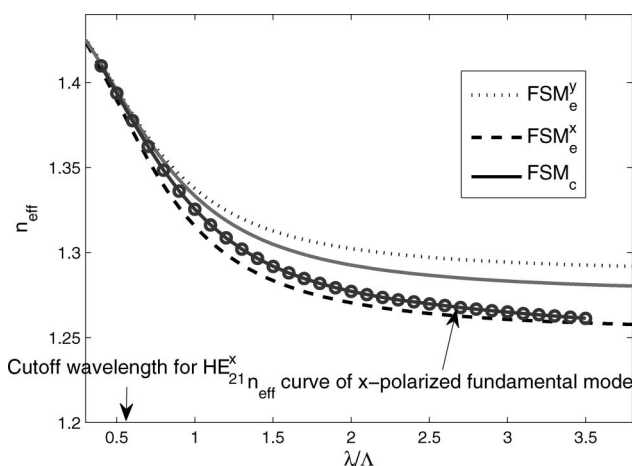We used 18 rings of elliptical airholes around the core region with a perfectly matched layer absorbing

Fig. 8. Effective index of the x-polarized fundamental core of the HE_{11}^x mode (filled circles curve), the FSM curve of the circular airhole core FSM_c (solid curve), and the two orthogonal nondegenerate FSM curves of the elliptical airhole cladding FSM_e^x and FSM_e^y (dotted and dashed curves, respectively). The structural parameters of the PCF are $d_c/\Lambda = 0.63$, $d_y/\Lambda = 0.9$, and $\eta = 2$.
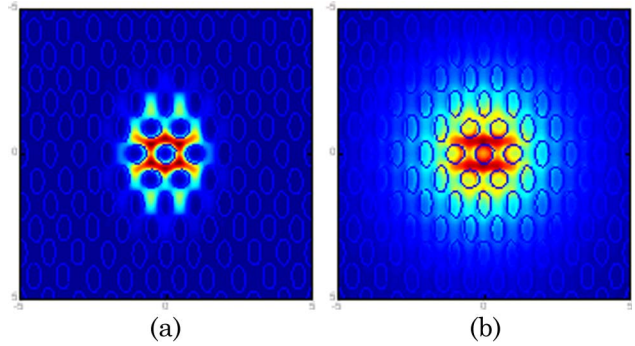

Fig. 9. (Color online) Field distribution of the E_x component of the x-polarized fundamental mode HE_{11}^x at (a) $\lambda/\Lambda = 0.5$ and (b) $\lambda/\Lambda = 1.4$.

boundary conditions to simulate the infinite microstructured cladding. Because of this finite thickness in the calculation, the fundamental guided mode is leaky. We estimated the confinement loss of the guided mode by using

$$\text{loss(dB/m)} = \frac{2\pi}{\lambda}\frac{20}{\ln 10}\text{Im}(n_{\text{eff}}).$$

Figure 10 presents the calculated confinement loss of the guided HE_{11}^x mode that increases drastically over a long wavelength range. We used $\Lambda = 1\,\mu m$ for the calculation. The confinement loss is of the order of (dB/m), which is high compared with the transmission fiber. To improve the confinement, we increased the number of circular airholes in the core region, e.g., from the current structure to more rings of airholes. The effective reduction of confinement loss especially at long wavelengths can be seen in Fig. 10. The minimum loss for the x-polarized fundamental mode is 3.9 dB/m for the PCF structure with one ring of circular airholes in the core region and approximately 0.48 dB/m for the PCF structure with two rings of airholes in the core region. For a fiber
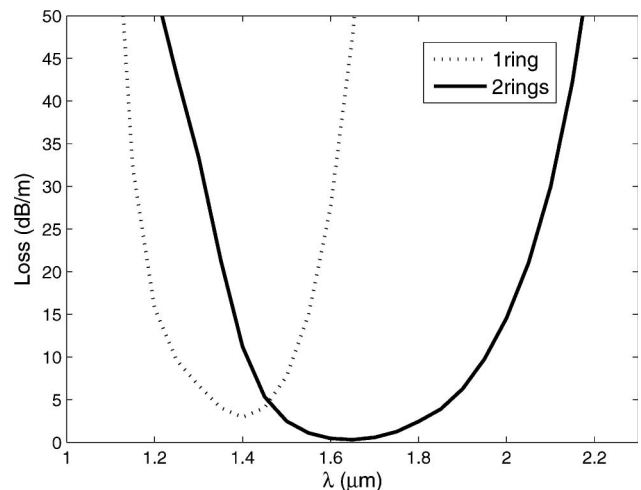

Fig. 10. Confinement loss of the HE_{11}^x mode in the proposed PCF structure with one ring of airholes in the core region (dotted curve) and two rings of airholes in the core region (solid curve).
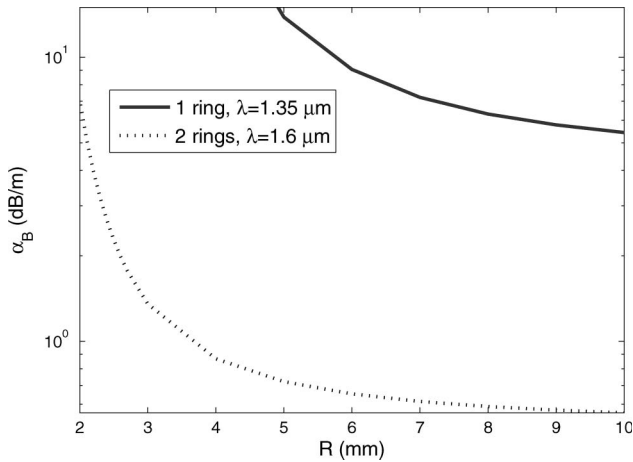
Fig. 11. Bending loss of the PCF structure with one ring of airholes in the core region at $\lambda = 1.35\,\mu$m (solid curve) and two rings of airholes in the core region at $\lambda = 1.6\,\mu$m (dotted curve) as a function of bending radius.

Fig. 12. Bending loss of the PCF structure with a bending radius of $5\,\mu$m. The loss curves represent one ring of airholes in the core region (solid curve), and two rings of airholes in the core region (dotted curve) as a function of wavelength.

structure with two rings of airholes in the core region, we used 17 rings of elliptical airholes in the fiber cladding so that the whole microstructured structure is the same size. Moreover, the bandwidth for confinement loss less than $5\,$dB/m is significantly broadened with two rings of airholes, and the wavelength corresponding to the lowest loss value moves to longer wavelengths, i.e., from 1.35 to $1.6\,\mu$m. It should be noted that the proposed fiber structure can be fabricated by the stack-and-draw method or multicapillary drawing method [23]. In solid core PCFs, absorption and Rayleigh scattering in the bulk glass can be the main sources of loss. In the proposed structure where the airholes are introduced to the core region, the air–silica interface roughness also causes scattering loss. The surface roughness could result from the fiber drawing process.

The bending property of the holey fiber is investigated by the FEM in which the bent fiber is represented by a straight fiber with an equivalent index profile [24]. We evaluated the bending loss as a function of bending radius for the proposed PCF structure as shown in Fig. 11. The solid curve represents the bending loss calculated for the PCF structure with one ring of circular airholes in the core region at $\lambda = 1.35\,\mu$m; the dotted curve represents the PCF structure with two rings of airholes in the core region at $\lambda = 1.6\,\mu$m. The wavelength values were chosen to represent where minimum confinement loss occurs for the structure. The bending loss decreases by approximately 1 order of magnitude at the same bending radius from a one-ring core to a two-ring core with better confinement. Figure 12 presents the bending loss of the fiber with a one-ring core and a two-ring core as a function of wavelength with the same bending radius of $5\,$mm. We also determined that the two-ring core PCF performs better than the one-ring core PCF in terms of the minimum bending loss value at the same bending radius and the wavelength range below a fixed bending loss.
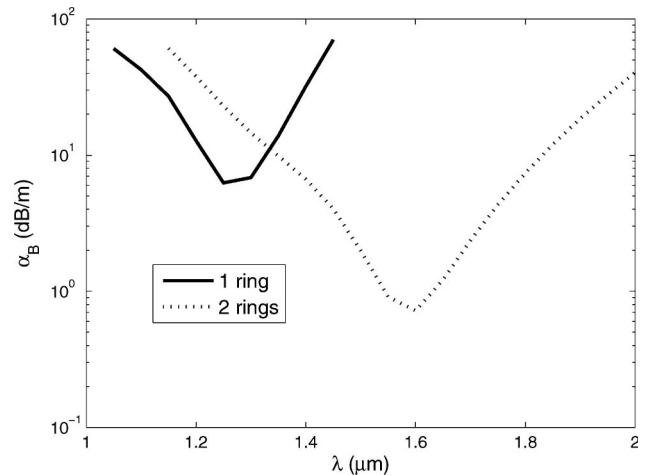
3. Conclusions

We have proposed a novel PCF structure with elliptical airholes in the cladding and circular airholes in the core region to achieve single-polarization single-mode operation. The structural geometry can be carefully designed to guide only one polarization state of the fundamental mode. The effects of structural parameters on cutoff wavelength and single-polarization operating range were discussed. The confinement loss can be reduced by the addition of more airholes to the core region. We also studied the bending properties of the PCF structure. The results proved that additional airholes in the core region could significantly suppress bending loss.

References

1. M.-J. Li, X. Chen, D. A. Nolan, G. E. Berkey, J. Wang, W. A. Wood, and L. A. Zenteno, "High bandwidth single polarization fiber with elliptical central air hole," J. Lightwave Technol. **23**, 3454–3460 (2005).
2. T. Okoshi and K. Oyamada, "Single-polarization single-mode optical fiber with refractive-index pits on both sides of the core," Electron. Lett. **16**, 712–713 (1980).
3. J. R. Simpson, R. H. Stolen, F. M. Sears, W. Pleibel, J. B. MacChesney, and R. E. Howard, "A single-polarization fiber," J. Lightwave Technol. **1**, 370–374 (1983).
4. K. S. Chiang, "Stress-induced birefringence fibers designed for single-polarization single-mode operation," J. Lightwave Technol. **7**, 436–441 (1989).
5. K. Tajima, M. Ohashi, and Y. Sasaki, "A new single-polarization optical fiber," J. Lightwave Technol. **7**, 1499–1503 (1989).
6. S. Furukawa, T. Fujimoto, and T. Hinata, "Propagation characteristics of a single-polarization optical fiber with an elliptic core and triple-clad," J. Lightwave Technol. **21**, 1307–1312 (2003).
7. T. A. Birks, C. Knight, and P. St. J. Russell, "Endlessly single-mode photonic crystal fiber," Opt. Lett. **22**, 961–963 (1997).

8. J. C. Knight, J. Arriaga, T. A. Birks, A. Ortigosa-Blanch, W. J. Wadsworth, and P. St. J. Russell, "Anomalous dispersion in photonic crystal fiber," IEEE Photon. Technol. Lett. **12**, 807–809 (2000).

9. K. Suzuki, H. Kubota, S. Kawanishi, M. Tanaka, and M. Fujita, "Optical properties of a low-loss polarization-maintaining photonic crystal fiber," Opt. Express **9**, 676–680 (2001).

10. T. P. Hansen, J. Broeng, S. E. B. Libori, E. Knudsen, A. Bjarklev, J. R. Jensen, and H. Simonsen, "Highly birefringent index-guiding photonic crystal fibers," IEEE Photon. Technol. Lett. **13**, 588–590 (2001).

11. M. J. Steel, T. P. White, C. M. de Sterke, R. C. McPhedran, and L. C. Botten, "Symmetry and degeneracy in microstructured optical fibers," Opt. Lett. **26**, 488–490 (2001).

12. M. Szpulak, J. Olszewski, T. Martynkien, W. Urbanńczyk, and J. Wojcik, "Polarizing photonic crystal fibers with wide operation range," Opt. Commun. **239**, 91–97 (2004).

13. K. Saitoh and M. Koshiba, "Single-polarization single-mode photonic crystal fibers," IEEE Photon. Technol. Lett. **15**, 1384–1386 (2003).

14. H. Kubota, S. Kawanishi, S. Koyanagi, M. Tanaka, and S. Yamaguchi, "Absolutely single polarization photonic crystal fiber," IEEE Photon. Technol. Lett. **16**, 182–184 (2004).

15. J. R. Folkenberg, M. D. Nielsen, and C. Jakobsen, "Broadband single-polarization photonic crystal fiber," Opt. Lett. **30**, 1446–1448 (2005).

16. J. Ju, W. Jin, and M. S. Demokan, "Design of single-polarization single-mode photonic crystal fiber at 1.30 and 1.55 μm," J. Lightwave Technol. **24**, 825–830(2006).

17. F. Zhang, M. Zhang, X. Liu, and P. Ye, "Design of wideband single-polarization single-mode photonic crystal fiber," J. Lightwave Technol. **25**, 1184–1189 (2007).

18. A. Argyros and N. Issa, "Microstructured optical fiber for single-polarization air guidance," Opt. Lett. **29**, 20–22 (2004).

19. M. Szpulak, T. Martynkien, J. Olszewski, W. Urbanńczyk, T. Nasilowski, F. Berghmans, and H. Thienpont, "Single-polarization single-mode photonic band gap fiber," Acta Phys. Pol. A **111**, 239–245 (2007).

20. K. K. Y. Lee, Y. Avniel, and S. G. Johnson, "Design strategies and rigorous conditions for single-polarization single-mode waveguides," Opt. Express **16**, 15170–15184 (2008).

21. M. Eguchi and Y. Tsuji, "Single-mode single-polarization holey fiber using anisotropic fundamental space-filling mode," Opt. Lett. **32**, 2112–2114 (2007).

22. M. Eguchi and Y. Tsuji, "Design of single-polarization elliptical-hole core circular-hole holey fibers with zero dispersion at 1.55 μm," J. Opt. Soc. Am. B **25**, 1690–1701 (2008).

23. J. C. Knight, T. A. Birks, P. St. J. Russell, and D. M. Atkin, "All-silica single-mode optical fiber with photonic crystal cladding," Opt. Lett. **21**, 1547–1549 (1996).

24. D. Marcuse, "Influence of curvature on the losses of doubly clad fibers," Appl. Opt. **21**, 4208–4213 (1982).